Dalton Transactions

Electrolytic Synthesis of Porphyrinic Zr Metal-Organic Frameworks with Selective Crystal Topologies

Journal:	*Dalton Transactions*
Manuscript ID	DT-COM-02-2021-000491.R1
Article Type:	Communication
Date Submitted by the Author:	15-Mar-2021

Complete List of Authors:	Okada, Keito; Kwansei Gakuin University, Department of Chemistry, School of Science and Technology Tanaka, Yoko; Kwansei Gakuin University, Department of Chemistry, School of Science and Technology Inose, Tomoko; Hokkaido University, RIES; Kyoto University, WPI-iCeMS Uji-i, Hiroshi; Hokkaido University, Research Institute for Electronics Scince (RIES); KU Leuven, Chemistry Yoshikawa, Hirofumi; Kwansei Gakuin University, Department of Nanotechnology for Sustainable Energy, School of Science and Technology; Kyoto University, KUIAS iCeMS Tanaka, Daisuke; Kwansei Gakuin University, Department of Chemistry, School of Science and Technology; JST, PRESTO

COMMUNICATION

Electrolytic Synthesis of Porphyrinic Zr-Metal–Organic Frameworks with Selective Crystal Topologies

Received 00th January 20xx,
Accepted 00th January 20xx

DOI: 10.1039/x0xx00000x

Keito Okada,[a] Yoko Tanaka,[a] Tomoko Inose,[b,c] Hiroshi Ujii,[b,d] Hirofumi Yoshikawa,[e] and Daisuke Tanaka*[a,f]

The thermodynamic (PCN-222) and kinetic (PCN-224) products of porphyrinic Zr-metal–organic frameworks (MOFs) were synthesized via an anodic dissolution approach for the first time. To the best of our knowledge, this is the first report of MOF polymorphs being controlled by electrolysis. The selective formation of PCN-222 requires an amorphous component to be present on the electrode during the initial reaction process.

Recently, the electrochemical synthesis of metal–organic frameworks (MOFs) has attracted considerable attention as a promising industrial method because it allows the *in situ* deposition of MOFs onto conductive surfaces.[1–3] Various MOFs have been synthesized using both anodic dissolution[4–10] and cathodic deposition approaches.[7,11–16] In particular, Zr(IV)-based MOFs have been widely investigated due to their high chemical and thermal stabilities.[17] Ameloot et al. reported the electrochemical deposition of UiO-66 films, which are prototypal Zr-MOFs, onto the surfaces of anodes and cathodes.[18] However, there are numerous difficulties in the electrochemical synthesis of Zr-MOFs, because the clusters formed by zirconium are largely affected by slight changes in the reaction conditions, such as concentration, reaction temperature, and reaction time. In particular, the addition of a carboxylic acid modulator is known to be effective for selectively forming clusters.[17,19] In addition, controlling the various crystal topologies (polymorphs) and defects of Zr-MOFs is a central research topic in this area of chemistry.[17] Generally, electrolytic reactions are interfacial heterogeneous reactions that proceed near the electrodes. The reactivity of the substrates in an electrolytic reaction differs from that of substrates in conventional bulk reactions because the precursor is not homogeneously distributed in the reaction cell but rather localized near the electrode.[20] Therefore, an approach for controlling the MOF topologies in an electrolytic reaction has not yet been completely elucidated, leaving room for further investigation.

Herein, we have investigated the electrochemical synthesis of porphyrinic Zr-MOFs on an electrode surface. These MOFs are highly stable and exhibit excellent photocatalytic properties, which originate from the porphyrin ligand; viz., tetrakis(4-carboxyphenyl)porphyrin (H_4TCPP).[17,21] Crystals of Zr-MOFs can exist in different topologies depending on the reaction conditions. In particular, porphyrinic Zr-MOFs with Zr_6O_8 nuclei can exist in at least six different topologies.[22–27] Generally, the obtained crystal topology depends on the various experimental parameters used during the crystal growth process.[22,28–35] Recently, the correlation between the topologies and the experimental parameters of porphyrinic Zr-MOF syntheses was systematically investigated by the solution-stirring method, and the effects of temperature and reaction time on the

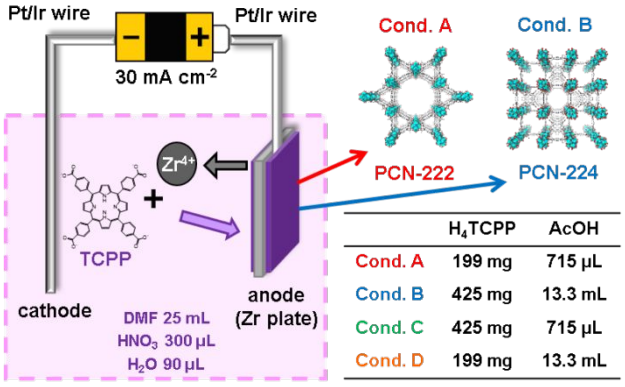

	H_4TCPP	AcOH
Cond. A	199 mg	715 µL
Cond. B	425 mg	13.3 mL
Cond. C	425 mg	715 µL
Cond. D	199 mg	13.3 mL

Fig. 1 Schematic illustration for the synthesis of porphyrinic Zr-metal–organic frameworks (MOFs) via electrolysis. The table shows the concentration conditions that were used to yield PCN-222 and PCN-224.

[a] Department of Chemistry, School of Science and Technology, Kwansei Gakuin University, 2-1 Gakuen, Sanda, Hyogo 669-1337, Japan.
[b] Research Institute for Electronic Science (RIES), Hokkaido University, N20W10, Sapporo 001-0020, Japan
[c] Institute for Integrated Cell-Material Sciences (WPI-iCeMS), Kyoto University, Yoshida, Sakyo-ku, Kyoto 606-8501, Japan
[d] Department of Chemistry, KU Leuven, Celestijnenlaan 200F, Heverlee, 3001, Belgium
[e] Department of Nanotechnology for Sustainable Energy, School of Science and Technology, Kwansei Gakuin University, Sanda, Hyogo 669-1337,
[f] Japan JST PRESTO, 2-1 Gakuen, Sanda, Hyogo 669-1337, Japan
*Corresponding Author. E-mail: dtanaka@kwansei.ac.jp.
Electronic Supplementary Information (ESI) available: Experimental information and additional data. See DOI: 10.1039/x0xx00000x

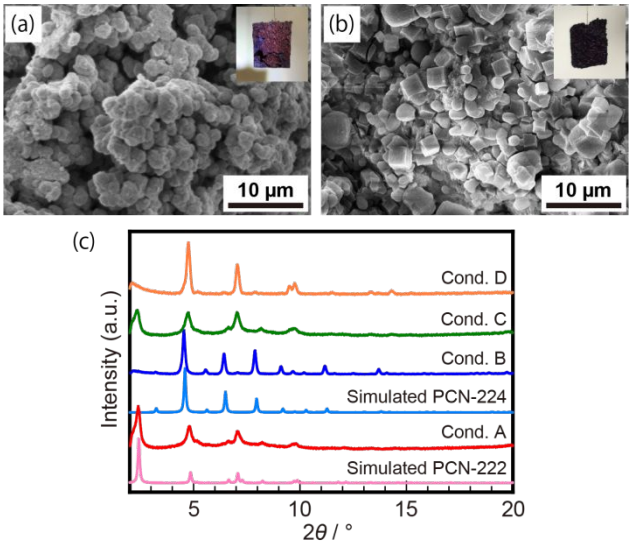

Fig. 2. Scanning electron microscopy (SEM) images and photographs of the synthesized anode substrate under conditions (a) A and (b) B. (c) Powder X-ray diffraction (PXRD) patterns of the crystals obtained under conditions A through D.

crystal phases were reported.[36] Although porphyrinic Zr-MOFs have been synthesized via the electrophoretic deposition (EPD) method, which employs both synthesis and deposition processes,[37] the *in situ* electrochemical deposition of porphyrinic Zr-MOFs by a facile one-step synthesis has not yet been accomplished. Moreover, there are no reports on the selective production of MOF crystal topologies via electrolysis. In this study, we used an anodic dissolution approach to synthesize Zr-MOFs and determined the synthetic conditions required to yield the thermodynamic product PCN-222/MOF-545 (**csq** topology) and the kinetic product PCN-224 (**she** topology) (Fig. 1).[23,25,27,36] To the best of our knowledge, this is the first report of MOF polymorphs being controlled by electrolysis. In particular, the formation of PCN-222 is preceded by the formation of an amorphous component during the initial stages of electrolysis.

The synthetic conditions used in this study are similar to those used for electrochemical UiO-66 film deposition[18] but with slight modifications. A Zr plate (1×1 cm^2, thickness: 0.2 mm) welded to a Pt/Ir wire was used as the anode, while another Pt/Ir wire was used as the cathode. A ligand solution was prepared by dissolving H_4TCPP in *N*,*N*-dimethylformamide (DMF). Acetic acid (AcOH) was added as a modulator, while water and nitric acid were used as additives to enhance the crystallinity of the product. The two electrodes were immersed in the ligand solution and heated to 110 °C under a nitrogen atmosphere and a constant current of 30 mA for 2 h. The crystalline compound obtained under condition A, which employed low ligand and modulator concentrations, was different from the compound formed under condition B, which used high ligand and modulator concentrations (see the table in Fig. 1). The same reactions were carried out at 60 °C under conditions A and B, but no crystalline compound was obtained in either case (see note S3 in the ESI). Furthermore, crystals could not be obtained without the applied current (see note S4 in the ESI). This suggests that the generation of Zr(IV) ions by electrolysis is crucial for the formation of crystalline compounds.

Under conditions A and B, purple and dark purple crystals, respectively, were obtained on both sides of the anode. Scanning electron microscopy (SEM) observations of the synthesized anode substrate under each condition showed that spherical polycrystals and cubic crystals were formed under conditions A and B, respectively (Figs. 2a and b). These two types of crystals were peeled off of the substrate and then characterized by powder X-ray diffraction (PXRD) measurements (Figs. 2c and S4). The PXRD patterns revealed that the purple crystals formed under condition A were PCN-222[25] and the dark purple crystals formed under condition B were PCN-224.[23] However, there is a possibility of MOF-525[27] (**ftw** topology) also forming under condition B because its simulation pattern is similar to that of PCN-224.[36] In addition, the PXRD patterns of the crystals precipitated in the solution (Fig. S5) revealed the low crystallinity of PCN-222 precipitated under condition A and suggested that a mixture of Zr-MOFs with different crystal topologies (NU-902[22] with **scu** topology and PCN-223[24] with **shp** topology) was formed in the solution under condition B. Subsequently, the properties of the pores of the crystals deposited on the anode substrates were evaluated by nitrogen gas adsorption measurements performed at 77 K (see note S6 in the ESI). The purple crystals produced under condition A showed a type-IV isotherm, while the dark purple crystals yielded under condition B followed a type-I isotherm. The shapes of the adsorption isotherms are identical to those previously reported for PCN-222 and PCN-224.[23,25] Thus, PXRD and nitrogen sorption isotherms verified that two types of porphyrinic Zr-MOF crystal topologies were selectively synthesized via electrolysis. However, the reported Brunauer–Emmett–Teller (BET) surface areas of PCN-222 and PCN-224 are 2200 $m^2\ g^{-1}$ and 2600 $m^2\ g^{-1}$, respectively, while the BET surface areas of our crystals obtained under conditions A and B are 419 $m^2\ g^{-1}$ and 2093 $m^2\ g^{-1}$, respectively.[23,25] The crystals obtained under condition A had low crystallinity, suggesting the presence of non-porous impurities. However, the crystallinity of PCN-222 was improved by additional heating after electrolysis (see note S7 in the ESI). This suggests that there is a good possibility that the crystallinity can be improved by further optimizing the synthetic conditions to include extended heating times.

Previous reports have indicated that PCN-222 is the thermodynamic product and PCN-224 is the kinetic product.[36] Considering the precursor concentrations used in this study, lower ligand and modulator concentrations promoted the formation of the thermodynamic product, while higher concentrations afforded the kinetic product. This observation is strikingly different from those made during conventional synthetic techniques, wherein the thermodynamic products were more likely to be obtained in the presence of high concentrations of strongly binding modulators.[38] Furthermore, compared to that of PCN-224, the formation of PCN-222 during bulk synthesis is facilitated in the presence of high porphyrin concentrations under conventional solvothermal synthesis condition.[23,25] Thus, the phenomenon involved in the electrolytic process seems to significantly differ from that observed in conventional bulk syntheses. Therefore, we investigated the

mechanism responsible for the formation of PCN-222 and PCN-224 under the different electrolysis conditions.

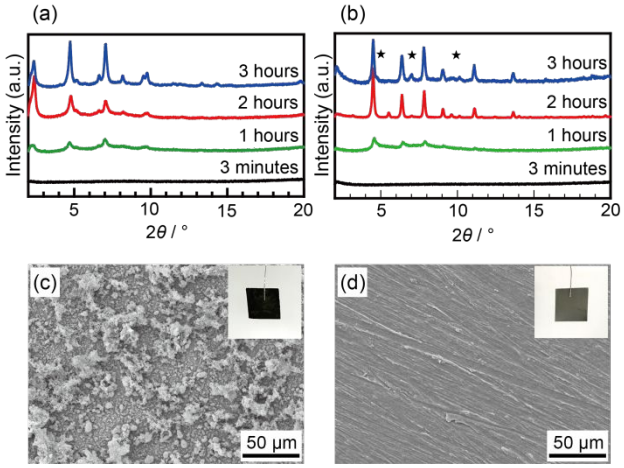

Fig. 3. PXRD patterns of time modulation for (a) condition A and (b) condition B. SEM images and photographs of the as-synthesized anode substrates after 3 min of electrolysis under (c) condition A and (d) condition B.

To elucidate the reaction mechanism, time modulation experiments were performed under each concentration condition. The formation of PCN-222 and PCN-224 was investigated using PXRD at different reaction times: 3 min, 1 h, and 3 h. Materials that formed on the substrates after 3 min were characterized as is, while those formed after 1 h were peeled off of the substrate prior to PXRD analysis. The PXRD patterns of the time modulation for conditions A and B are shown in Figs. 3a, 3b, S8, and S9. Under condition A, the crystallinity of the product, PCN-222, improved with time. Under condition B, peaks corresponding to PCN-224 were observed in the samples obtained after 1 h and 2 h. However, a shoulder appeared at approximately 5° and new peaks were observed at approximately 7° and 10° in the PXRD pattern of the crystals formed after 3 h. The positions of the new peaks were identical to the diffraction angles of the major peaks of the NU-902 and PCN-223 crystal topologies (Fig. S9), indicating that under condition B, a mixture of Zr-MOFs with different crystal topologies (NU-902 and PCN-223) was yielded with increasing time.

The SEM images and photographs of the substrates obtained under each condition revealed that at a reaction time of 3 min, purple deposits were only observed on the anode under condition A, while the anode substrate remained unchanged under condition B (Figs. 3c and d). The PXRD patterns of the substrates obtained under each condition showed no clear diffraction peaks (Figs. 3a, b; S8; and S9). Therefore, Raman spectroscopy was conducted to analyze the surface states of the anodes. The results obtained after 3 min and 2 h under each condition are shown in Fig. S10 and Table S6 (see note S9 in the ESI). Under condition A, a porphyrin-derived vibration was observed from the substrate formed after 3 min and 2 h, indicating that the porphyrin-derived material was immediately deposited after applying a current under condition A. By contrast, deposition did not occur in the initial stages of the reaction under condition B. This difference in the deposition phenomena possibly arises from the modulator concentration present in condition B being higher than that in condition A, resulting in impeded porphyrin aggregation

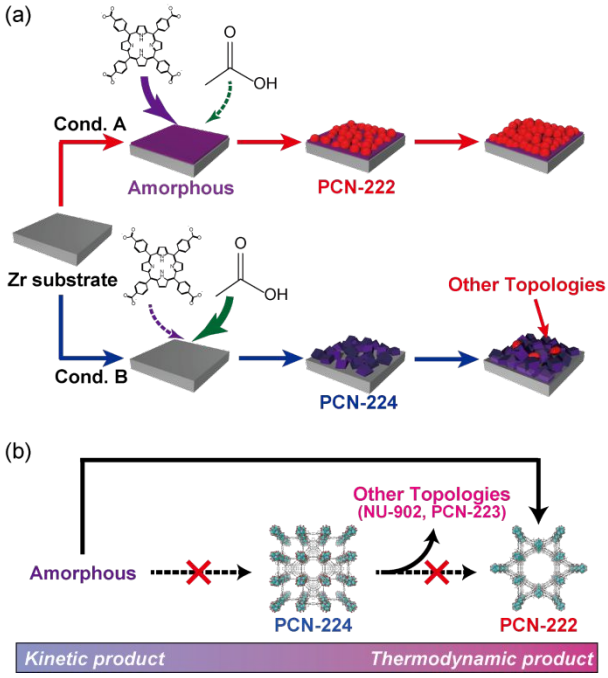

Fig. 4. (a) Proposed mechanism for the deposition of MOFs with PCN-222 and PCN-224 topologies. (b) Kinetic and thermodynamic relationships, along with the changes in the crystal phases of the compounds obtained after electrolysis.

under the former and successful aggregation under the latter.

Futhermore, additional experiments were performed to investigate the effects of ligand and modulator concentrations on the crystal phase changes of porphyrinic Zr-MOFs formed by electrolytic synthesis. To accomplish this, electrolytic synthesis was carried out under two other sets of conditions: Condition C, which employed the same amount of modulator as that used in condition A and the same ligand concentration as that in condition B; and condition D, which used the same amount of modulator as that used in condition B and the same ligand concentration as that in condition A (see the table in Fig. 1). The crystals obtained on the anode under these two conditions were subsequently analyzed by PXRD (Figs. 2c and S4). The PXRD patterns showed that PCN-222 was formed under condition C, where only the ligand was added in large amounts (similar to condition A). On the other hand, under condition D, where only a large amount of modulator was added, a mixture of various crystal topologies, such as PCN-222, PCN-223, and PCN-224, was formed. Therefore, it is suggested that the amount of modulator contributes more than the ligand concentration to the different MOF crystal topologies formed during electrolytic synthesis.

Based on these results, we propose that the mechanism for PCN-222 and PCN-224 formation on the anode proceeds as shown in Fig. 4a. Under condition A, the amorphous, porphyrin-derived component, which was deposited immediately after applying a current, gradually changes to afford PCN-222, whose crystallinity improves with increasing reaction time. Nucleation of the thermodynamically stable PCN-222 does not occur directly on the substrate; instead, PCN-222 is formed by heating the amorphous phase present on the substrates for a certain time period. This

presumption is consistent with the low specific surface area of the synthesized PCN-222. On the other hand, as mentioned earlier, under condition B, the high AcOH concentration near the anode hinders the approach of porphyrin toward the Zr(IV) ions. Thus, the deposition of amorphous components is inhibited during the initial stages. However, after sufficient time, the Zr(IV)-ion concentration increases and the ions are able to react with the porphyrin ligands approaching the interface to form crystalline PCN-224 nuclei. This initiates the growth of PCN-224 crystals, which are more thermodynamically stable than the amorphous components. However, over time, a mixture is obtained as the generated PCN-224 gradually transforms into other, even more thermodynamically stable crystal topologies. These findings indicate that the amorphous component is the kinetically-favored compound, PCN-222 is the most thermodynamically stable, and PCN-224 is an intermediate compound (Fig. 4b). Thus, the selective synthesis of thermodynamically stable PCN-222 was achieved via the formation of a kinetic, amorphous compound at the electrode interface. On the other hand, by adding a large amount of modulator, the low-crystalline amorphous-phase formation was hindered, while the highly crystalline PCN-224 was deposited directly onto the anode.

Conclusions

Two types of porphyrinic Zr-MOF crystal topologies were successfully synthesized for the first time via an anodic dissolution approach, wherein a Zr plate was used as the anode. The thermodynamic product, PCN-222, was obtained under low ligand and modulator concentrations, and the kinetic product, PCN-224, was obtained under high concentrations. These concentration conditions differed from those used in bulk synthesis. The mechanism for the formation of both MOFs was investigated by time modulation experiments. These experiments revealed that under low modulator concentrations, the kinetically-favored, amorphous component is initially deposited and then gradually transforms into PCN-222, the most thermodynamically stable MOF. On the other hand, under high modulator concentrations, PCN-224, which is more thermodynamically stable than the amorphous component, is directly produced onto the anode surface and converts to various other thermodynamically stable phases over time. In this study, we demonstrated that the interfacial reactions, and consequently the MOF crystal topologies, can be successfully controlled by modifying the reaction conditions. These findings may assist the development of an electrolytic process for precise MOF synthesis. In addition, this study encourages the development of other novel methods for fabricating various crystalline porphyrinic Zr-MOFs. Furthermore, since past literature has reported that the formation of zirconium oxide competes with the electrolytic synthesis of UiO-66,[18] the effect of the presence of zirconium oxide on the crystallinity and selectivity of Zr-MOF synthesis is currently being investigated.

Acknowledgements

This work was supported by JST PRESTO (Grant No. JPMJPR17NA) and JSPS KAKENHI (Grant Nos. 20H02577, 17H03003, 20K21165, 20K05413, 19KK0136, 20H04646, and 20H04680). This work was performed under the Cooperative Research Program of "Network Joint Research Center for Materials and Devices."

Conflicts of interest

There are no conflicts to declare.

References

1. W.-J. Li, M. Tu, R. Cao and R. A. Fischer, *J. Mater. Chem. A*, 2016, **4**, 12356.
2. M. Rubio-Martinez, C. Avci-Camur, A. W. Thornton, I. Imaz, D. Maspoch and M. R. Hill, *Chem. Soc. Rev.*, 2017, **46**, 3453.
3. X. Zhang, K. Wan, P. Subramanian, M. Xu, J. Luo and J. Fransaer, *J. Mater. Chem. A*, 2020, **8**, 7569.
4. R. Ameloot, L. Stappers, J. Fransaer, L. Alaerts, B. F. Sels and D. E. De Vos, *Chem. Mater.*, 2009, **21**, 2580.
5. N. Campagnol, E. R. Souza, D. E. De Vos, K. Binnemans and J. Fransaer, *Chem. Commun.*, 2014, **50**, 12545.
6. N. Campagnol, T. Van Assche, T. Boudewijns, J. Denayer, K. Binnemans, D. De Vos and J. Fransaer, *J. Mater. Chem. A*, 2013, **1**, 5827.
7. N. Campagnol, T. R. C. Van Assche, M. Li, L. Stappers, M. Dincă, J. F. M. Denayer, K. Binnemans, D. E. De Vos and J. Fransaer, *J. Mater. Chem. A*, 2016, **4**, 3914.
8. A. Martinez Joaristi, J. Juan-Alcañiz, P. Serra-Crespo, F. Kapteijn and J. Gascon, *Cryst. Growth Des.*, 2012, **12**, 3489.
9. S. D. Worrall, H. Mann, A. Rogers, M. A. Bissett, M. P. Attfield and R. A. W. Dryfe, *Electrochim. Acta*, 2016, **197**, 228.
10. H. M. Yang, X. L. Song, T. L. Yang, Z. H. Liang, C. M. Fan and X. G. Hao, *RSC Adv.*, 2014, **4**, 15720.
11. S. Alizadeh and D. Nematollahi, *J. Am. Chem. Soc.*, 2017, **139**, 4753.
12. M. Li and M. Dinca, *J. Am. Chem. Soc.*, 2011, **133**, 12926.
13. M. Li and M. Dincă, *Chem. Sci.*, 2014, **5**, 107.
14. M. Li and M. Dincă, *Chem. Mater.*, 2015, **27**, 3203.
15. F. Zhang, Y. Wang, T. Chu, Z. Wang, W. Li and Y. Yang, *Analyst*, 2016, **141**, 4502.
16. Q. Zhang, Z. Wu, Y. Lv, Y. Li, Y. Zhao, R. Zhang, Y. Xiao, X. Shi, D. Zhang, R. Hua, J. Yao, J. Guo, R. Huang, Y. Cui, Z. Kang, S. Goswami, L. Robison, K. Song, X. Li, Y. Han, L. Chi, O. K. Farha and G. Lu, *Angew. Chem., Int. Ed. Engl.*, 2019, **58**, 1123.
17. Y. Bai, Y. Dou, L. H. Xie, W. Rutledge, J. R. Li and H. C. Zhou, *Chem. Soc. Rev.*, 2016, **45**, 2327.
18. I. Stassen, M. Styles, T. Van Assche, N. Campagnol, J. Fransaer, J. Denayer, J.-C. Tan, P. Falcaro, D. De Vos and R. Ameloot, *Chem. Mater.*, 2015, **27**, 1801.
19. T. Tsuruoka, S. Furukawa, Y. Takashima, K. Yoshida, S. Isoda and S. Kitagawa, *Angew. Chem., Int. Ed. Engl.*, 2009, **48**, 4739.
20. T. Fuchigami, S. Inagi and M. Atobe, *Fundamentals and*

Applications of Organic Electrochemistry, John Wiley & Sons, Ltd, 2015.
21. W. Y. Gao, M. Chrzanowski and S. Ma, *Chem. Soc. Rev.*, 2014, **43**, 5841.
22. P. Deria, D. A. Gomez-Gualdron, I. Hod, R. Q. Snurr, J. T. Hupp and O. K. Farha, *J. Am. Chem. Soc.*, 2016, **138**, 14449.
23. D. Feng, W. C. Chung, Z. Wei, Z. Y. Gu, H. L. Jiang, Y. P. Chen, D. J. Darensbourg and H. C. Zhou, *J. Am. Chem. Soc.*, 2013, **135**, 17105.
24. D. Feng, Z. Y. Gu, Y. P. Chen, J. Park, Z. Wei, Y. Sun, M. Bosch, S. Yuan and H. C. Zhou, *J. Am. Chem. Soc.*, 2014, **136**, 17714.
25. D. Feng, Z. Y. Gu, J. R. Li, H. L. Jiang, Z. Wei and H. C. Zhou, *Angew. Chem., Int. Ed. Engl.*, 2012, **51**, 10307.
26. H. L. Jiang, D. Feng, K. Wang, Z. Y. Gu, Z. Wei, Y. P. Chen and H. C. Zhou, *J. Am. Chem. Soc.*, 2013, **135**, 13934.
27. W. Morris, B. Volosskiy, S. Demir, F. Gandara, P. L. McGrier, H. Furukawa, D. Cascio, J. F. Stoddart and O. M. Yaghi, *Inorg. Chem.*, 2012, **51**, 6443.
28. D. Banerjee, J. Finkelstein, A. Smirnov, P. M. Forster, L. A. Borkowski, S. J. Teat and J. B. Parise, *Cryst. Growth Des.*, 2011, **11**, 2572.
29. V. Bon, I. Senkovska, I. A. Baburin and S. Kaskel, *Cryst. Growth Des.*, 2013, **13**, 1231.
30. S. J. Garibay, I. Iordanov, T. Islamoglu, J. B. DeCoste and O. K. Farha, *CrystEngComm*, 2018, **20**, 7066.
31. T. Islamoglu, K.-i. Otake, P. Li, C. T. Buru, A. W. Peters, I. Akpinar, S. J. Garibay and O. K. Farha, *CrystEngComm*, 2018, **20**, 5913.
32. D. Kim, X. Song, J. H. Yoon and M. S. Lah, *Cryst. Growth Des.*, 2012, **12**, 4186.
33. G.-X. Liu, H. Xu, H. Zhou, S. Nishihara and X.-M. Ren, *CrystEngComm*, 2012, **14**, 1856.
34. H. Noh, C.-W. Kung, T. Islamoglu, A. W. Peters, Y. Liao, P. Li, S. J. Garibay, X. Zhang, M. R. DeStefano, J. T. Hupp and O. K. Farha, *Chem. Mater.*, 2018, **30**, 2193.
35. T. E. Webber, W. G. Liu, S. P. Desai, C. C. Lu, D. G. Truhlar and R. L. Penn, *ACS Appl. Mater. Interfaces*, 2017, **9**, 39342.
36. X. Gong, H. Noh, N. C. Gianneschi and O. K. Farha, *J. Am. Chem. Soc.*, 2019, **141**, 6146.
37. I. Hod, M. D. Sampson, P. Deria, C. P. Kubiak, O. K. Farha and J. T. Hupp, *ACS Catal.*, 2015, **5**, 6302.
38. O. M. Yaghi, M. J. Kalmutzki and C. S. Diercks, *Introduction to Reticular Chemistry: Metal‐Organic Frameworks and Covalent Organic Frameworks*, Wiley‐VCH Verlag GmbH & Co. KGaA, 2019.

